Shell effect in the mean square charge radii and magnetic moments of bismuth isotopes near $N = 126$

A. E. Barzakh,* D. V. Fedorov, V. S. Ivanov, P. L. Molkanov, F. V. Moroz, S. Yu. Orlov, V. N. Panteleev, M. D. Seliverstov, and Yu. M. Volkov
Petersburg Nuclear Physics Institute (PNPI), NRC Kurchatov Institute, Gatchina 188300, Russia

(Received 23 November 2017; published 31 January 2018)

Isotope shift relative to ^{209}Bi and hyperfine splitting for ^{211,213}Bi have been measured by in-source laser spectroscopy at the 306.77-nm atomic transition. The pronounced shell effect both in radii and magnetic moments in Bi isotopes at $N = 126$ has been observed. The isotopic trend of magnetic moment for $9/2^-$ ground states of even-N Bi isotopes has been qualitatively explained by the change in the first-order core-polarization correction. The possible influence of the octupole degree of freedom on the magnetic moment behavior at $N > 126$ has been discussed.

DOI: 10.1103/PhysRevC.97.014322

I. INTRODUCTION

The shell effect in the changes of the nuclear mean-square charge radius $\delta\langle r^2\rangle$—the kink in its isotopic trend at the magic neutron numbers—was found to be a universal feature of the $\delta\langle r^2\rangle$ behavior [1]. The characteristic change in the slope of the $\delta\langle r^2\rangle$ isotopic dependencies is observed at $N = 28$, 50, 82, 126 [1]. The theoretical attempts to describe this effect were concentrated primarily on the Pb isotopic chain near $N = 126$. It was shown by Sharma *et al.* [2] and Tajima *et al.* [3] that the standard nonrelativistic Hartree-Fock (HF) approach fails to explain this effect. At the same time, the kink in radii trend is well explained in the relativistic mean-field (RMF) calculations [2] (see also Refs. [4–6], where the description of the shell effect at the other neutron magic numbers by the RMF was presented). It was claimed by Reinhard and Flocard [7] and Sharma *et al.* [2] that the difference between the HF and RMF results is determined by the difference in the isovector spin-orbit force in these approaches. Correspondingly, by a modification of the spin-orbit contribution to the nonrelativistic Skyrme functional, Reinhard and Flocard introduced the new forces SkI3 and SkI4, which reproduce the kink at ^{208}Pb [7].

The quality of the shell-effect description in the RMF and HF approaches correlates with the population of the $\nu i_{11/2}$ orbital beyond $N = 126$ [8]. The increase of the $\nu i_{11/2}$-orbital occupancy in the RMF and modified HF approaches was shown to be connected with the decrease of the energy splitting between the $\nu g_{9/2}$ and $\nu i_{11/2}$ levels in contradiction with the experimental evidences [8]. Recently Nakada and Inakura [9] succeeded in reproducing the $\delta\langle r^2\rangle$ behavior for the Pb nuclei in the Hartree-Fock-Bogoliubov calculations with the density-dependent spin-orbit interaction derived from the chiral three-nucleon interaction by Kohno [10]. The rapid increase of the charge radius at $N > 126$ was described fairly well in the framework of this approach without the convergence of the $\nu g_{9/2}$ and $\nu i_{11/2}$ levels [9].

It was shown also that the kink may be not solely due to the spin-orbit interaction but could be due to a density-dependent pairing interaction as well (see Refs. [3,11]).

Thus, additional experimental data are of importance to choose between the different theoretical explanations.

Unfortunately, experimental data on the shell effect in radii near $N = 126$ are limited to the $_{82}$Pb isotopic chain [12]. There are indications of the presence of this effect also in $_{83}$Bi, $_{84}$Po, $_{86}$Ra, $_{87}$Fr, $_{88}$Rn, and $_{89}$Ac chains [1,13], but all of them are based on the interpolation of the $\delta\langle r^2\rangle$ values between $N = 126$ and $N = 130$ or 132, since there are no corresponding data for the $N = 128$ nuclei. However, the further we go from the magic $N = 126$, the more significant become contributions to $\delta\langle r^2\rangle$ due to other effects (vibration, deformation, etc.). Therefore, to extract the "pure" shell effect, it is preferable to have the data for the nuclei nearest to the shell closure. In the case of the even-N Bi isotopes, it is the ^{211}Bi$_{128}$ nucleus. The measurement of the $\delta\langle r^2\rangle_{209,211}$ value is one of the aims of the present work.

Magnetic moments (μ) for the odd-Z, even-N nuclei also display regular behavior when crossing the neutron magic numbers. For example, the magnetic moments of the $\pi d_{5/2}$ Eu ground states reach maximum at the neutron shell closure with the near linear isotopic dependence on both sides of the magic number $N = 82$ [14] (cf. also data for Tb [$\pi s_{1/2}$], Ref. [15], and Pm [$\pi d_{5/2}$], Ref. [16] at $N > 82$). The similar behavior of the magnetic moments of the $9/2^-$ ($\pi h_{9/2}$) ground states was found in the Bi isotopes [17,18].

The magnetic moment of ^{211}Bi$_{128}$ was measured by the nuclear orientation method in Ref. [19]: $\mu(^{211}\text{Bi}) = 3.80(13)\,\mu_N$. However, there is a discrepancy between nuclear-orientation (NO) [20] and laser-spectroscopy (LS) [18] results for adjacent even-N ^{213}Bi : $\mu(^{213}\text{Bi},\ NO) = 3.89(9)\,\mu_N$, $\mu(^{213}\text{Bi},\ \text{LS}) = 3.672(7)\,\mu_N$. Similar discrepancy (~6%) exists for ^{206}Bi used as a reference nucleus in the NO experiments [19–21]. The possible additional uncertainty of 6% leads to the value $\mu(^{211}\text{Bi}) = 3.80(36)\,\mu_N$. In the limits of the revised

*barzakh@mail.ru

uncertainty the shell effect in the $\mu(9/2^-;\,\mathrm{Bi})$ values at $N = 126$ almost disappears: cf. $\mu(^{209}\mathrm{Bi}_{126}) = 4.1103(5)\,\mu_N$ [22,23]. To elucidate the behavior of the Bi ground-state magnetic moments immediately after $N = 126$, $\mu(^{211}\mathrm{Bi}_{128})$ has been measured in the present work with the reduced uncertainty.

II. EXPERIMENTAL DETAILS

In-source laser spectroscopy was used for bismuth isotope shift (IS) and hyperfine structure (hfs) measurements. Experiments were performed at the laser-nuclear complex of the Investigation of Radioactive Isotopes on Synchrocyclotron (IRIS) facility working on line with a 1-GeV proton beam of the Petersburg Nuclear Physics Institute synchrocyclotron [24].

Radioactive Bi isotopes were produced in spallation reactions by 1-GeV protons in a uranium monocarbide target. The spallation products diffused out of the target material as neutral atoms and effused into the hot cavity of the ion source. Laser beams were introduced into this cavity. The lasers were tuned to perform three-step resonance ionization of Bi atoms [25].

The photoion current was measured via the detection of α decays of the isotopes in question as a function of the scanned laser frequency of the first excitation step ($6p^3\,{}^4S_{3/2} \rightarrow 6p^2\,7s\,{}^4P_{1/2}$, 306.77 nm). The example of experimental spectra is presented in Fig. 1.

The detailed description of the laser setup and the experimental procedure can be found in Refs. [24,25].

III. RESULTS

The data were analyzed with a fixed hfs a-constants ratio $a(6p^3\,{}^4S_{3/2})/a(6p^2\,7s\,{}^4P_{1/2}) = -11.0101(13)$ [18,26]. For ^{213}Bi the quadrupole hyperfine constant b was fixed: $b(6p^3\,{}^4S_{3/2};\ {}^{213}\mathrm{Bi}) = -491(25)$ MHz [18].

The magnetic dipole moments were calculated using the standard scaling relation with ^{209}Bi as a reference,

$$\mu_A = \mu_{\mathrm{ref}}\frac{a_A(6p^3\,{}^4S_{3/2})}{a_{\mathrm{ref}}(6p^3\,{}^4S_{3/2})}.$$

In this relation the hyperfine structure anomaly (HFA) is neglected. For the isotopes with the same odd-nucleon configuration and nearly equal magnetic moments, the HFA is of order $10^{-3} - 10^{-4}$ [27]. This is the case for ^{209,211,213}Bi ($\pi h_{9/2}$ configuration). The following reference values were used: $a_{209}({}^4S_{3/2}) = -446.937(1)$ MHz [26], $\mu_{209} = 4.1103(5)\,\mu_N$ [22,23].

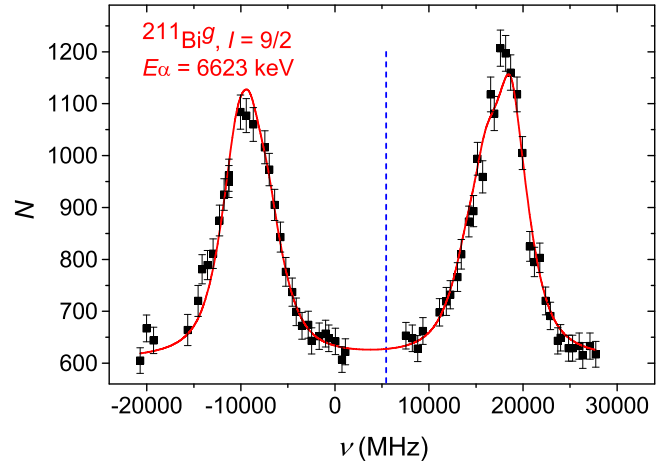

FIG. 1. The hfs spectrum of ^{211}Bi. The spin and the energy of the α-decay line used for the photoion current monitoring are shown. The solid line depicts the Voigt-profile fit to the data. The vertical dashed line marks the centroid of the hfs. The zero point on the frequency scale corresponds to the centroid of the reference ^{209}Bi hfs.

The electric quadrupole moment Q_A of the isotope with atomic number A was calculated using the relation

$$Q_A = \frac{b_A}{b_{209}}Q_{209},$$

where $b_{209} = -305.067(2)$ MHz [26] and $Q_{209} = -0.420(8)$ b [28].

The hyperfine constants, isotope shifts, magnetic dipole moments, electric quadrupole moments, and changes in the mean-square charge radii for ^{211,213}Bi are presented in Table I. Isotope shift and the a-constant value for the long-lived ^{213}Bi, measured in the present work, are in agreement with the more precise data obtained by the gas-cell method [18] (see Table I).

The changes in the mean-square charge radii were deduced from the measured isotope shift $\delta\nu^{A,A'}$ using the relations

$$\begin{aligned}\delta\nu^{A,A'} &= \delta\nu_F^{A,A'} + \delta\nu_M^{A,A'},\\ \delta\nu_F^{A,A'} &= F\delta\langle r^2\rangle_{A,A'},\\ \delta\nu_M^{A,A'} &= \frac{M(A-A')}{AA'},\end{aligned} \tag{1}$$

where $\delta\nu_F^{A,A'}$ and $\delta\nu_M^{A,A'}$ are the field and mass shifts, F is an electronic factor, $M = M^{\mathrm{NMS}} + M^{\mathrm{SMS}}$, M^{NMS} and M^{SMS} are normal mass shift and specific mass shift (SMS)

TABLE I. Isotope shifts, hfs constants, changes in the mean-square charge radii, magnetic and quadrupole moments for ^{213,211}Bi.

A	$\delta\nu_{209,A}$ (MHz)	a (MHz)	b (MHz)	$\delta\langle r^2\rangle_{209,A}$ (fm^2)[a]	μ (μ_N)	Q (b)
211	5490(150)	−419.9(3.1)	−410(200)	0.221(6){15}	3.862(29)	−0.57(28)
213	10630(230)	−397(8)	−491[b]			
213	10507(24)[c]	−399.3(1.8)[c]	−491(25)[c]	0.422(1){29}	3.672(7)	−0.68(5)

[a]The errors in parentheses are the statistical experimental uncertainties. The systematic errors are given in the curly brackets and stem from the uncertainty of the F and M factors.
[b]This value was fixed during the fitting.
[c]Reference [18].

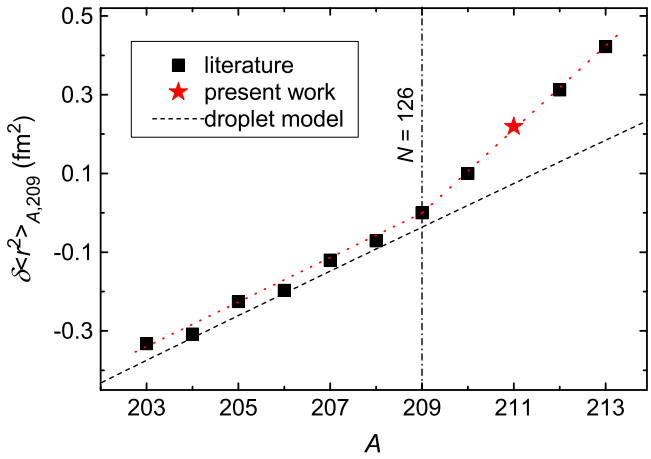

FIG. 2. Changes in the mean-square charge radii for Bi isotopes near the shell closure at $N = 126$. Star: present work; squares: Ref. [18]. The experimental points are connected by dotted line to guide the eyes. Dashed line shows the droplet model predictions.

constants, respectively. The electronic factor was estimated in Ref. [25] using the systematics of $\delta\langle r^2\rangle$ in the Pb region: $F(Bi;\ 306.77\,\mathrm{nm}) = 24.8(17)\,\mathrm{GHz\,fm^{-2}}$. The specific mass shift is usually small for this type of transition ($p \to s$), and one can assume $M = (1 \pm 2)\,M^{\mathrm{NMS}}$ (cf. similar relations for analogous transitions in adjacent atoms [29–31]).

IV. CHANGES IN MEAN-SQUARE CHARGE RADII

A. Shell effect

In Fig. 2 changes in the mean-square charge radii $\delta\langle r^2\rangle$ for the Bi nuclei near $N = 126$ are shown along with the droplet-model predictions [32].

To compare the shell effect in different isotopic chains we introduced the dimensionless parameter ξ_{even}:

$$\xi_{\mathrm{even}} \equiv \frac{\delta\langle r^2\rangle_{128,126}}{\delta\langle r^2\rangle_{126,124}} = \frac{\delta\nu^{\mathrm{FS}}_{128,126}}{\delta\nu^{\mathrm{FS}}_{126,124}}.$$

Lower indices point to the neutron numbers. This parameter is independent of the uncertainties of the F factor (usually 5−10% in the lead region). The choice of the even-N isotope nearest to the neutron magic numbers helps to avoid mixing of the shell effect with other effects which might contribute to the observed $\delta\langle r^2\rangle$ value.

It is instructive also to consider the shell effect for the odd-N isotopes:

$$\xi_{\mathrm{odd}} \equiv \frac{\delta\langle r^2\rangle_{127,126}}{\delta\langle r^2\rangle_{125,124}} = \frac{\delta\nu^{\mathrm{FS}}_{127,126}}{\delta\nu^{\mathrm{FS}}_{125,124}}.$$

In Table II parameters ξ_{even} and ξ_{odd} for different isotopic chains in the Pb region are presented. The comparison of the $\delta\langle r^2\rangle_{N,N'}$ values for $N,N' = 126,\ 125$ and $N,N' = 127,\ 126$ also shows the shell effect [33], i.e., the increase of $\delta\langle r^2\rangle$ when going across the neutron shell. However, when one compares $\delta\langle r^2\rangle$ for different Z the systematic uncertainties stemming from the electronic factor F should be taken into account. Besides, in this case the shell effect is mixed with the odd-even staggering effect. In the presence of odd-even staggering the $\delta\langle r^2\rangle_{N,\,N+1}$ value (at even N) is usually less than the $\delta\langle r^2\rangle_{N-1,\,N}$ value independently on the shell effect. In contrast, the parameter ξ_{odd} is independent of the F-factor uncertainty, and choosing the pair $N,N' = 125,\ 124$ instead of the pair $N,N' = 126,\ 125$ enables one to minimize the influence of the odd-even staggering.

TABLE II. Shell-effect parameters.

Z	ξ_{even}	ξ_{odd}	References
81 (Tl)		1.97(49)[a]	[34]
82 (Pb)	1.79(2)	2.13(5)	[12]
83 (Bi)	1.83(7)	2.07(14)	[18] and the present work
84 (Po)		2.14(32)	[35–37]
87 (Fr)		2.45(21)[b]	[33,38]
		2.16(21)[c]	[33,38]

[a] $\delta\langle r^2\rangle_{122,123}$ was used instead of $\delta\langle r^2\rangle_{124,125}$.
[b] $I(^{214}\mathrm{Fr}_{127}) = 1$.
[c] $I(^{214}\mathrm{Fr}_{127}) = 2$.

The shell-effect parameters for Bi and Pb nuclei coincide in the limit of uncertainties (see Table II and Fig. 3). Theoretical RMF calculations overestimate ξ_{even} ([2,4–6]; see also Fig. 3). A better description of the shell effect for Pb nuclei was obtained recently with a new extended parametrization of the RMF model based on the effective field theory (see Fig. 2 in Ref. [39]) and in the relativistic Hartree-Fock theory with nonlinear terms and density-dependent meson-nucleon coupling [40,41]. The fair description of the shell effect is determined by the noticeable population of the $\nu i_{11/2}$ orbital due to the near degeneracy or even inverse ordering of the $\nu g_{9/2}$ and $\nu i_{11/2}$ shells in contradiction with the experimental evidences (see detailed analysis in Ref. [8]). The shell effect at $N = 126$ was described fairly well in the framework of the nonrelativistic approach with density-dependent spin-orbit interaction without the decrease of the energy splitting between the $\nu g_{9/2}$ and $\nu i_{11/2}$ levels [9]. However, in this approach the

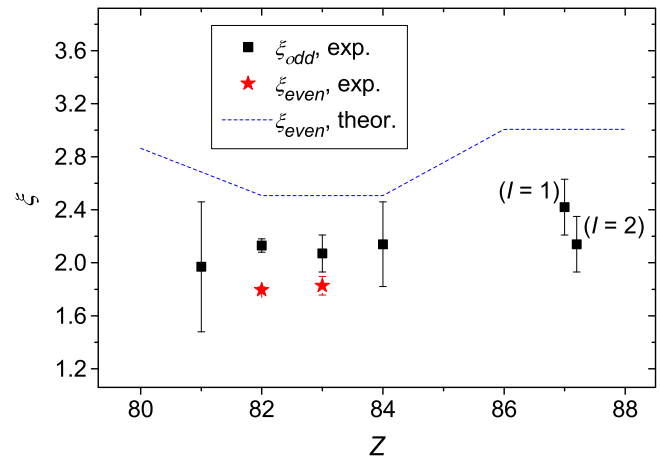

FIG. 3. Shell-effect parameters for the Pb-region nuclei. The sources of the experimental data are indicated in Table II. Dashed line shows the results of the RMF calculations [6].

noticeable population of the $\nu i_{11/2}$ orbital also plays a key role in reproducing the kink in the Pb-radii trend.

Thus, all theoretical studies require the noticeable occupancy of the $\nu i_{11/2}$ orbital for the nuclei with $N > 126$ in order to reproduce the shell effect in radii at $N = 126$. Even when the $\nu g_{9/2}$ orbital is bound deeper than the $\nu i_{11/2}$ orbital, the pairing interaction allows the scattering of enough Cooper pairs of neutrons into the $\nu i_{11/2}$ shell.

The shell-effect parameter $\xi_{\rm odd}$ proved to be comparable with that for the even-N nuclei, $\xi_{\rm even}$. This means that the shell effect for the nuclei with $N = 127$ is nearly the same as the shell effect for the even-N isotopes. However, the pairing mechanism of the $\nu i_{11/2}$-shell population does not work when we have only one neutron above the closed shell ($N = 127$).

It was assumed in Ref. [33] on the base of the magnetic moment analysis that the admixture of the $[\pi h_{9/2}, \nu i_{11/2}]_{1-}$ configuration to the leading $[\pi h_{9/2}, \nu g_{9/2}]_{1-}$ configuration in ^{214}Fr$_{127}$ is possible. In Refs. [42,43] the different configuration admixtures ($[\pi h_{9/2}, \nu i_{11/2}]_{1-}$ included) to the ground-state wave function of ^{210}Bi$_{127}$ were derived from the β-decay data. It was supposed in Ref. [33] that the presumed admixture of the configuration with the $i_{11/2}$ neutron may contribute to the shell effect for ^{214}Fr$_{127}$. However, this possibility is absent in the even-Z, odd-N nuclei (^{209}Pb, ^{211}Po) with the pure $\nu g_{9/2}$ configuration. Correspondingly, the $\nu i_{11/2}$ shell cannot play any role in the shell effect observed for these nuclei. Note that the parameter $\xi_{\rm odd}$ does not depend on Z, and there is no difference between $\xi_{\rm odd}$ for the odd-odd nuclei with the possible $\nu i_{11/2}$-state admixture and the even-Z nuclei where such an admixture is impossible (see Table II).

Theory does not reproduce the experimental results for the shell effect in the odd-N isotopes. This is clearly seen in Fig. 2 of Ref. [9] where the change in the $\delta\langle r^2\rangle$ slope in the Pb chain starts in theory after $N = 127$ rather than after $N = 126$ as in the experiment (that is, in theory $\xi_{\rm odd} \approx 1$, whereas $\xi_{\rm even} \approx 2$). See also Fig. 3 of Ref. [9] with zero theoretical $\nu i_{11/2}$-shell occupation probability at $N = 127$. The energy density functional method based on the theory of finite Fermi systems [11] also fails to reproduce $\xi_{\rm odd}$ at the reasonable description of $\xi_{\rm even}$ (see Figs. 5 and 6 in Ref. [11]). To summarize, the comparison of the experimental $\delta\langle r^2\rangle$ values for the odd-N nuclei in the close vicinity of the $N = 126$ shell closure with the theory casts doubts on the commonly accepted understanding of the nature of the shell effect in nuclear radii, implying the decisive role of the $\nu i_{11/2}$-shell occupation.

B. Odd-even staggering

The odd-even staggering refers to the fact that, generally, the isotope shift is smaller if a neutron is added to an even-N isotope than to an odd-N one. To estimate the odd-even staggering we used the parameter γ, introduced by Tomlinson and Stroke [44]:

$$\gamma_A = \frac{2\delta\langle r^2\rangle_{A-1,A}}{\delta\langle r^2\rangle_{A-1,A+1}}.$$

The measurement of $\delta\langle r^2\rangle_{209,211}$ enables us to determine γ_{127} and γ_{129} for Bi isotopes (see Fig. 4). Staggering parameters for Bi coincide in the limits of uncertainties with the corresponding γ's for Pb. In particular, they show the same subshell effect, i.e., the small jumps of the γ value at $N = 126$ and $N = 124$, indicating the onset of filling up of the various neutron orbitals.

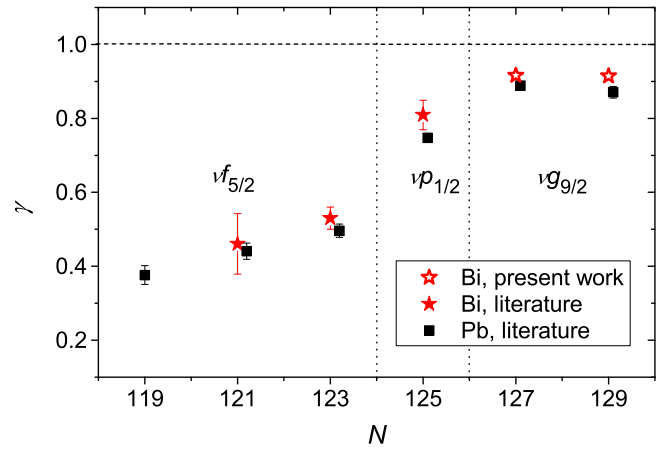

FIG. 4. Odd-even staggering parameter for Pb (squares, Ref. [12]), and Bi isotopes (hollow stars, present work; filled stars, Ref. [18]). Filling neutron subshells are shown.

V. MAGNETIC MOMENTS

The evolution of the magnetic moments of the $9/2^-$ ground states in Bi (see Refs. [17,18,25] and the present paper), Fr, [45–47] and Ac [48,49] isotopes near $N = 126$ reveals a striking similarity of the corresponding isotopic trends: the peak at the neutron shell closure with the linear isotopic dependence on both sides of the magic number $N = 126$ (see Fig. 5). The μ values for $9/2^-$ isomeric states in Tl also display the same behavior at $N < 126$ [50,51].

The large departure of the $\mu(^{209}\text{Bi})$ value [$4.1103(5)\,\mu_N$] from the Schmidt estimation [$\mu_{\rm Sch}(\pi h_{9/2}) = 2.62\mu_N$] is a long-standing nuclear-physics problem [52]. It was realized

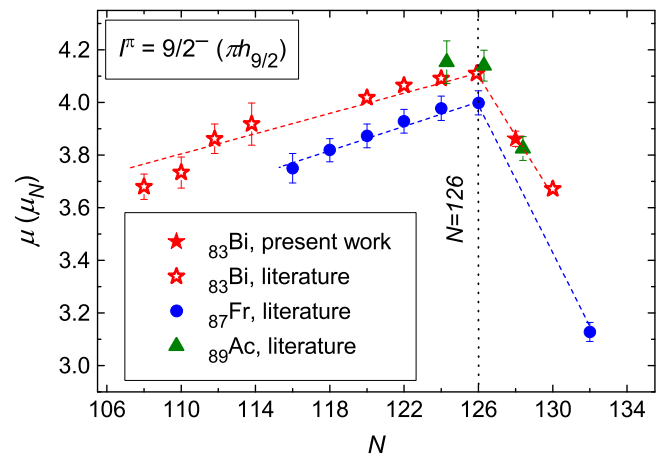

FIG. 5. Magnetic moments for $9/2^-$ ($\pi h_{9/2}$) ground states in Bi, Fr, and Ac isotopes. Filled star: ^{211}Bi, present paper. Hollow stars: Bi, Refs. [17,18,25]. Circles: Fr, Refs. [45–47]. Triangles: Ac, Refs. [48,49]. Points are connected by lines to guide the eyes.

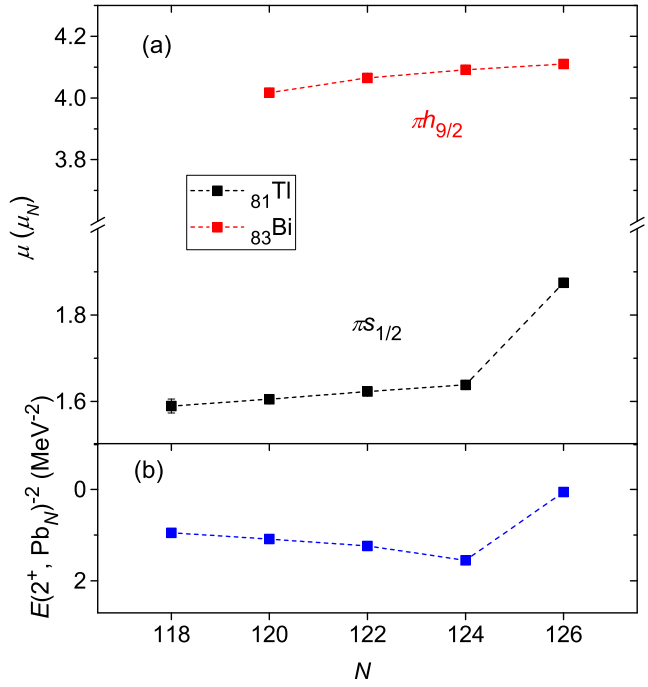

FIG. 6. (a) Isotopic dependencies of the magnetic moment for Bi (Ref. [18] and the present work) and Tl [57,58] ground states near $N = 126$. (b) $E(2^+)^{-2}$ for the core Pb nuclei [59]. Points are connected by lines to guide the eyes.

that this increase of the magnetic moment stems mainly from the contributions of the meson-exchange current ($\Delta\mu_{\rm mes}$) and the first-order ($\Delta\mu_{\rm CP1}$) and the second-order ($\Delta\mu_{\rm CP2}$) core-polarization corrections [52]. The meson-exchange process is expected to be essentially independent on the number of valence nucleons (though the corresponding correction depends on the particular configuration) [53].

The most important contribution in the second-order configuration mixing comes from the valence-nucleon coupling with the low-lying collective excited states of the core (2^+, 3^-, etc.) [54]. For example, the drop in the $\mu(5/2^-;\ \mathrm{Eu})$ values on both sides of the $N = 82$ shell closure correlates with the variation of the contribution due to the particle-vibration coupling which is expected to be roughly proportional to the $[E(2^+;\ \mathrm{Gd})]^{-2}$ value in the second-order perturbation theory (see Ref. [55]). Correspondingly, simple particle-core calculations explain the $\mu(5/2^-;\ \mathrm{Eu})$ drop rather well [55].

The same approach was successfully applied to the $1/2^+$ ($\pi s_{1/2}$) state in the Tl nuclei near $N = 126$ by Sagawa and Arima [56]. The jump in the Tl magnetic moment when going from $N = 124$ to $N = 126$ correlates with the jumplike behavior of the excitation energy of the first 2^+ core state (see Fig. 6). At the same time the $\mu(9/2^-;\ \mathrm{Bi})$ value changes smoothly at $N \leqslant 126$ and its isotopic dependency cannot be related to the second-order core-polarization correction due to a particle-(quadrupole)-vibration coupling.

Thus, the most probable source of the shell effect in the $9/2^-$ magnetic moments near $N = 126$ is the first-order core polarization. The same conclusion was drawn in Refs. [54,60,61] regarding the variation of $\mu(\nu i_{13/2})$ and $\mu(\nu f_{5/2})$ with neutron number at $N \leqslant 126$ (see also the calculations of the neutron-CP1 correction in Refs. [60,61]).

The configuration admixture contributing to the magnetic dipole moment in the first order of perturbation theory corresponds to the transition of a single particle from an orbit $j = l + 1/2$ to its spin-orbit partner $j = l - 1/2$ [62]. Near doubly magic ^{208}Pb, the most important are two such core excitations corresponding to proton $(h^{-1}_{11/2}h_{9/2})$ and neutron $(i^{-1}_{13/2}i_{11/2})$ particle-hole states. The proton-CP1 correction does not depend on the neutron number. At the same time, the increasing occupation probability of the $\nu i_{13/2}$ orbital gives rise to the increase of the neutron-CP1 correction with N. This causes the up-going trend of $\mu(\pi h_{9/2})$ at $N < 126$. At $N > 126$, the $\nu i_{11/2}$ orbital starts to be populated. As the result, the probability of the excitation of the $i_{13/2}$ neutron to the $i_{11/2}$ state decreases and, correspondingly, the neutron-CP1 correction decreases with N. Thus, the neutron-CP1 correction is maximal at $N = 126$ where the $\nu i_{13/2}$ orbital is completely filled and the $\nu i_{11/2}$ orbital is empty.

We estimated neutron-CP1 correction to show its relevance to the $\mu(\pi h_{9/2})$ isotopic dependencies.

According to Refs. [60,62]

$$\Delta\mu_{\rm CM1}(N) = C[(2j_1 + 1)v^2_{j_1}(N)][(2j_2 + 1)u^2_{j_2}(N)], \quad (2)$$

where $j_1 = 13/2$, $j_2 = 11/2$, and u and v are the occupation numbers, which are given in the BCS approximation by

$$v^2_j = \frac{1}{2}\left[1 - \frac{\varepsilon_j - \lambda}{\sqrt{(\varepsilon_j - \lambda)^2 + \Delta^2}}\right],\ v^2_j + u^2_j = 1,$$

where Δ is a shell gap, ε_j is a single-particle energy [63], and λ is a chemical potential determined by the equation

$$N = N_0 + \sum_n (2j_n + 1)v^2_{j_n} \quad (3)$$

with $N_0 = 82$. Summation in Eq. (3) is restricted to the neutron shells between $N = 82$ and $N = 126$ and six neutron shells above $N = 126$ ($2g_{9/2}$, $1i_{11/2}$, $1j_{15/2}$, $3d_{5/2}$, $4s_{1/2}$, $2g_{7/2}$).

In the magnetic moment calculation

$$\mu_{\rm calc}(N) = \mu_0 + \Delta\mu_{\rm CM1}(N) \quad (4)$$

we use the simplest constant shell-gap approximation [64,65],

$$\Delta = \frac{12}{\sqrt{A}}\mathrm{MeV} \approx 0.8\ \mathrm{MeV}.$$

At fixed μ_0, the coefficient C in Eq. (2) was chosen from the condition $\mu_{\rm calc}(126) = \mu_{\rm exp}(^{209}\mathrm{Bi})$. The parameter μ_0 was determined by the fit to the experimental μ values: $\mu_0 = 3.0\,\mu_N$. This μ_0 value corresponds well to the sum

$$\mu_{\rm Sch}(\pi h_{9/2}) + \Delta\mu_{\rm mes} = 3.1\mu_N,$$

where the meson exchange correction is taken from Ref. [66].

Calculations reproduce N dependence of the Bi magnetic moments at $N < 126$ fairly well (see Fig. 7). The kink at $N = 126$ also takes place although it is less pronounced than the experimental one. Similar to the case of the shell effect in radii, the shell effect in magnetic moments crucially depends on the relative position of the $\nu i_{11/2}$ and $\nu g_{9/2}$ orbitals: with the

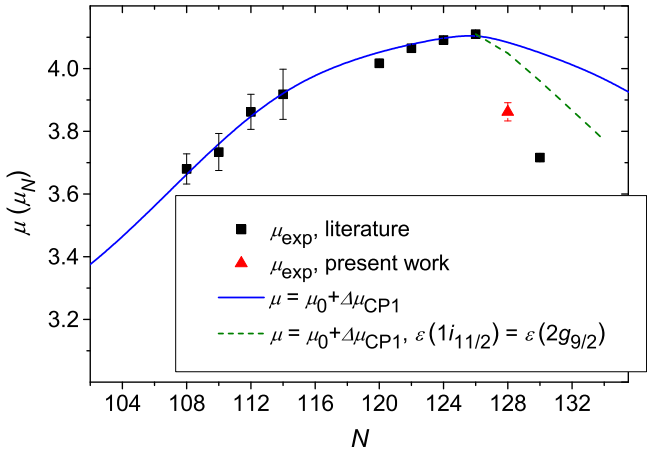

FIG. 7. Comparison of the experimental magnetic moments of the Bi isotopes (squares: Ref. [18]; triangle: present work) with the calculation by Eq. (2) [solid line: calculations with the experimental single-particle energies, Ref. [63]; dashed line: calculations with the assumption $\varepsilon(1i_{11/2}) = \varepsilon(2g_{9/2})$].

artificial assumption of their degeneracy, $\varepsilon(\nu i_{11/2}) = \varepsilon(\nu g_{9/2})$, calculated values become closer to the experimental data (Fig. 7).

However, even with the assumption $\varepsilon(\nu i_{11/2}) = \varepsilon(\nu g_{9/2})$, calculations noticeably underestimate the slope of the $\mu(9/2^-;\ \mathrm{Bi})$ isotopic dependency at $N > 126$. This discrepancy may be related to the possible CP2 correction due to the particle-(octupole)-vibration coupling. It is well known that the octupole degree of freedom plays an important role in the explanation of the $M1$ properties for the nuclei near ^{208}Pb (see, for example, Refs. [67,68] and references therein). Excitation energy of the lowest 3^- state in the core Pb nuclei is nearly constant for $N = 122-126$ and markedly decreases for $N = 128$ [69]. Calculations using a particle-vibration coupling model reproduce this behavior and predict the continuing decrease of the $E(3^-;\ \mathrm{Pb}_N)$ value for $N = 130, 132$ [68]. This may be regarded as an indication of the negligible octupole-CP2 contribution to the N dependence of the $\mu(9/2^-;\ \mathrm{Bi})$ value at $N < 126$ and the increase of this contribution at $N > 126$.

Considerable efforts were undertaken in recent years to formulate the fully self-consistent approach to the magnetic moment calculations in the framework of the relativistic mean-field [70,71] and finite Fermi system [72,73] theories. It would be instructive to test whether these more fundamental approaches will be able to describe the observed regular and universal behavior of the magnetic moments in the vicinity of ^{208}Pb.

VI. CONCLUSIONS

The measurement of the magnetic moment and the change in the mean-square charge radii for $^{211}\mathrm{Bi}_{128}$ allowed us to establish the shell effect in magnetic moments and radii in the closest vicinity of the neutron magic number $N = 126$.

Analysis of the radii shell-effect parameters ξ_{even} and ξ_{odd} for several isotopic chains in the Pb region revealed the independency of the shell effect at $N = 126$ on the proton number at the current level of the experimental accuracy. An adopted explanation of the shell effect in radii at $N = 126$ connects this effect with the increased population of the neutron $i_{11/2}$ orbital above the $N = 126$ shell closure. Observation of the noticeable shell effect also for $N = 127$ nuclei ($\xi_{\mathrm{odd}} \approx 2$) at $Z = 80-87$ casts doubts on this interpretation.

The regular behavior of the $\mu(9/2^-;\ \mathrm{Bi})$ values near $N = 126$ (linear decrease on the both sides of the magic number) was qualitatively explained by the neutron first-order core-polarization corrections. The faster decrease of the $\mu(9/2^-;\ \mathrm{Bi})$ values at $N > 126$ than at $N < 126$ may be attributed to the influence of the octupole degree of freedom.

[1] I. Angeli, Yu. P. Gangrsky, K. P. Marinova, I. N. Boboshin, S. Yu. Komarov, B. S. Ishkhanov, and V. V. Varlamov, J. Phys. G: Nucl. Part. Phys. **36**, 085102 (2009).
[2] M. M. Sharma, G. A. Lalazissis, and P. Ring, Phys. Lett. B **317**, 9 (1993).
[3] N. Tajima, P. Bonche, H. Flocard, P.-H. Heenen, and M. S. Weiss, Nucl. Phys. A **551**, 434 (1993).
[4] G. A. Lalazissis, S. Raman, and P. Ring, At. Data Nucl. Data Tables **71**, 1 (1999).
[5] M. Bender, P.-H. Heenen, and P.-G. Reinhard, Rev. Mod. Phys. **75**, 121 (2003).
[6] S. E. Agbemava, A. V. Afanasjev, D. Ray, and P. Ring, Phys. Rev. C **89**, 054320 (2014); see Supplemental Material at http://link.aps.org/supplemental/10.1103/PhysRevC.89.054320.
[7] P-G. Reinhard and H. Flocard, Nucl. Phys. A **584**, 467 (1995).
[8] P. M. Goddard, P. D. Stevenson, and A. Rios, Phys. Rev. Lett. **110**, 032503 (2013).
[9] H. Nakada and T. Inakura, Phys. Rev. C **91**, 021302(R) (2015).
[10] M. Kohno, Phys. Rev. C **88**, 064005 (2013).
[11] S. A. Fayans, S. V. Tolokonnikov, E. L. Trykov, and D. Zawischa, Nucl. Phys. A **676**, 49 (2000).
[12] M. Anselment *et al.*, Nucl. Phys. A **451**, 471 (1986).
[13] R. Ferrer *et al.*, Nat. Commun. **8**, 14520 (2017).
[14] S. A. Ahmad, W. Klempt, C. Ekstrom, R. Neugart, K. Wendt, and the ISOLDE Collaboration, Z. Phys. A **321**, 35 (1985).
[15] G. D. Alkhazov *et al.*, Z. Phys. A **337**, 367 (1990).
[16] G. D. Alkhazov *et al.*, J. Phys. B: At. Mol. Opt. Phys. **25**, 571 (1992).
[17] A. Barzakh *et al.*, Phys. Rev. C **95**, 044324 (2017).
[18] M. R. Pearson *et al.*, J. Phys. G: Nucl. Part. Phys. **26**, 1829 (2000).
[19] D. A. Williams *et al.*, Hyperfine Interact. C **1**, 565 (1996).
[20] M. Lindroos, P. Richards, J. Blomqvist, J. Rivovska, N. J. Stone, and the NICOLE and ISOLDE collaborations, Hyperfine Interact. **75**, 109 (1992).
[21] P. Herzog, K. Freitag, C. Herrmann, and K. Schlösser, Hyperfine Interact. **15/16**, 329 (1983).
[22] Y. Ting and D. Williams, Phys. Rev. **89**, 595 (1953).

[23] T. Baştuğ, B. Fricke, M. Finkbeiner, and W. R. Johnson, Z. Phys. D **37**, 281 (1996).
[24] A. Barzakh *et al.*, Rev. Sci. Instrum. **83**, 02B306 (2012).
[25] A. Barzakh *et al.*, Phys. Rev. C **94**, 024334 (2016).
[26] R. J. Hull and G. O. Brink, Phys. Rev. A **1**, 685 (1970).
[27] J. R. Persson, Atom. Data Nucl. Data Tables **99**, 62 (2013).
[28] T. Q. Teodoro and R. L. A. Haiduke, Phys. Rev. A **88**, 052504 (2013).
[29] G. Ulm *et al.*, Z. Phys. A: At. Nucl. **325**, 247 (1986).
[30] W. H. King and M. Wilson, J. Phys. G: Nucl. Part. Phys. **11**, L43 (1985).
[31] B. Cheal, T. E. Cocolios, and S. Fritzsche, Phys. Rev. A **86**, 042501 (2012).
[32] D. Berdichevsky and F. Tondeur, Z. Phys. A: At. Nucl. **322**, 141 (1985).
[33] G. J. Farooq-Smith *et al.*, Phys. Rev. C **94**, 054305 (2016).
[34] A. Barzakh *et al.*, Phys. Rev. C **88**, 024315 (2013).
[35] D. Kowalewska *et al.*, Phys. Rev. A **44**, R1442(R) (1991).
[36] T. E. Cocolios *et al.*, Phys. Rev. Lett. **106**, 052503 (2011).
[37] M. D. Seliverstov *et al.*, Phys. Lett. B **719**, 362 (2013).
[38] H. T. Duong *et al.*, Europhys. Lett. **3**, 175 (1987).
[39] B. Kumar, S. K. Singh, B. K. Agrawal, and S. K. Patra, Nucl. Phys. A **966**, 197 (2017).
[40] W. Long, J. Meng, N. Van Giai, and S.-G. Zhou, Phys. Rev. C **69**, 034319 (2004).
[41] W. Long, N. Van Giai, and J. Meng, arXiv:nucl-th/0608009v4.
[42] L. Szybisz, Nucl. Phys. A **244**, 107 (1975).
[43] H. Behrens and L. Szybisz, Nucl. Phys. A **223**, 268 (1974).
[44] W. J. Tomlinson and H. H. Stroke, Nucl. Phys. **60**, 614 (1964).
[45] I. Budinčević *et al.*, Phys. Rev. C **90**, 014317 (2014).
[46] R. P. de Groote *et al.*, Phys. Rev. Lett. **115**, 132501 (2015).
[47] K. M. Lynch *et al.*, Phys. Rev. X **4**, 011055 (2014).
[48] D. Decman *et al.*, Nucl. Phys. A **436**, 311 (1985).
[49] C. Granados *et al.*, Phys. Rev. C **96**, 054331 (2017).
[50] G. Neyens, Rep. Prog. Phys. **66**, 633 (2003).
[51] A. Barzakh *et al.*, Phys. Rev. C **95**, 014324 (2017).
[52] A. Arima, K. Shimizu, W. Bentz, and H. Hyuga, Adv. Nucl. Phys. **18**, 1 (1987), and references therein.
[53] M. Chemtob, Nucl. Phys. A **123**, 449 (1969).
[54] J. Wouters, N. Severijns, J. Vanhaverbeke, and L. Vanneste, J. Phys. G: Nucl. Part. Phys. **17**, 1613 (1991).
[55] K. Heyde, Hyperfine Interact. **75**, 69 (1992).
[56] A. Arima and H. Sagawa, Phys. Lett. **173**, 351 (1986).
[57] R. Neugart *et al.*, Phys. Rev. Lett. B **55**, 1559 (1985).
[58] N. J. Stone, At. Data Nucl. Data Tables **90**, 75 (2005).
[59] B. Pritychenko, M. Birch, B. Singh, and M. Horoi, At. Data Nucl. Data Tables **107**, 1 (2016).
[60] C. Roulet *et al.*, Nucl. Phys. A **285**, 156 (1977).
[61] C. Stenzel, H. Grawe, H. Haas, H.-E. Mahnke, and K. H. Maier, Nucl. Phys. A **411**, 248 (1983).
[62] A. Arima and H. Horie, Prog. Theor. Phys. **11**, 509 (1954).
[63] N. Schwierz, I. Wiedenhöver, and A. Volya, arXiv:0709.3525.
[64] J. Jänecke, T. W. O'Donnell, and V. I. Goldanskii, Nucl. Phys. A **728**, 23 (2003).
[65] P. Möller and J. R. Nix, Nucl. Phys. A **229**, 269 (1974).
[66] A. Arima and L. J. Huang-Lin, Phys. Lett. B **41**, 429 (1972).
[67] A. E. Stuchbery, A. P. Byrne, G. D. Dracoulis, B. Fabricius, and T. Kibédi, Nucl. Phys. A **555**, 355 (1993).
[68] I. Hamamoto, Nucl. Phys. A **155**, 362 (1970).
[69] T. Kibédi and R. H. Spear, At. Data Nucl. Data Tables **80**, 35 (2002).
[70] J. M. Yao, H. Chen, and J. Meng, Phys. Rev. C **74**, 024307 (2006).
[71] J. Li, J. X. Wei, J. N. Hu, P. Ring, and J. Meng, Phys. Rev. C **88**, 064307 (2013).
[72] I. N. Borzov, E. E. Saperstein, and S. V. Tolokonnikov, Phys. At. Nucl. **71**, 469 (2008).
[73] I. N. Borzov, E. E. Saperstein, S. V. Tolokonnikov, G. Neyens, and N. Severijns, Eur. Phys. J. A **45**, 159 (2010).